From antiferromagnetism to high-T_c weak ferromagnetism manipulated by atomic rearrangement in Ba3NiOs2O9

Hai L. Feng (冯海) [1,2,*] Jie Chen (陈洁),[3,4,†] Zhiwei Hu,[1] Xiao Wang,[1] Manfred Reehuis,[5] Peter Adler [1] Andreas Hoser,[5] Mei-Xia Wu,[6] Stefano Agrestini,[1,7] Hari Babu Vasili [7] J. Herrero-Martin [7] Lucie Nataf,[8] Francois Baudelet,[8] Kai Chen,[5] Yoshitaka Matsushita [9] Man-Rong Li [6] Liu Hao Tjeng [1] Claudia Felser [1] Martin Jansen [1,10] and Kazunari Yamaura[3,4]

[1]*Max Planck Institute for Chemical Physics of Solids, Dresden D-01187, Germany*
[2]*Beijing National Laboratory for Condensed Matter Physics, Institute of Physics, Chinese Academy of Sciences, Beijing 100190, China*
[3]*International Center for Materials Nanoarchitectonics (WPI-MANA), National Institute for Materials Science, Tsukuba 305-0044, Japan*
[4]*Graduate School of Chemical Science and Engineering, Hokkaido University, Sapporo 060-0810, Japan*
[5]*Helmholtz-Zentrum Berlin für Materialien und Energie, Hahn-Meitner-Platz 1, 14109 Berlin, Germany*
[6]*Key Laboratory of Bioinorganic and Synthetic Chemistry of Ministry of Education, School of Chemistry,*
Sun Yat-Sen University, Guangzhou 510275, China
[7]*ALBA Synchrotron Light Source, E-08290 Cerdanyola del Vallès, Barcelona, Spain*
[8]*Synchrotron SOLEIL, L'Orme des Merisiers, Saint-Aubin, 91192 Gif-sur-Yvette Cedex, France*
[9]*Materials Analysis Station, National Institute for Materials Science, Tsukuba, Ibaraki 305-0047, Japan*
[10]*Max Planck Institute for Solid State Research, Stuttgart D-70569, Germany*

Polycrystalline samples of Ba3NiOs2O9 were synthesized at ambient pressure (AP) and high pressure (HP) conditions, respectively. Both samples are electrically semiconducting. The AP Ba3NiOs2O9 crystallizes in the 6*H* perovskite structure with space group $P6_3/mmc$, consisting of face-sharing Os2O9 dimer units and corner-sharing NiO6 octahedra. Magnetic measurements indicated that AP Ba3NiOs2O9 is antiferromagnetically ordered below 130 K. HP Ba3NiOs2O9 crystallizes in the 6*H* perovskite structure too, but the face-sharing octahedral sites appear to be occupied by both Ni^{2+} and Os^{5+} ions, whereas the corner-sharing site is occupied exclusively by Os^{5+}. HP Ba3NiOs2O9 undergoes a high-temperature (≈ 400 K) weak ferromagnetic transition, which is much different from the antiferromagnetism of the AP phase. The long-range magnetic order of HP Ba3NiOs2O9 was confirmed by neutron powder diffraction. X-ray magnetic circular dichroism analysis supported ferromagnetic coupling between Os and Ni moments which leads to a spin arrangement, where the ferromagnetic moments mainly arise from Ni^{2+} ions.

I. INTRODUCTION

Transition metal oxides (TMOs) in which the electrons are correlated show various phenomena, e.g., colossal magnetoresistance [1], metal-insulator transitions, high-temperature superconductivity [2], Weyl semimetal and quantum spin-liquid behavior [3], as well as various kinds of magnetism like high-temperature ferro/ferrimagnetic (FM/FIM) transitions in insulators or half metals [4–6]. Triple perovskite oxides, Ba3BB'_2O9, usually adopt six-layered-hexagonal (6*H*) BaTiO3 related structures. For example, 6*H* Ba3BB'_2O9 ($B =$ Li, Na, Mg, Ca, Sr, Ti, Fe, Ni, Co, Cu, Zn, Zr, Bi, or a

lanthanide; $B' =$ Ru, Ir, Sb, Os) were reported, in which there are corner-sharing octahedral BO_6 sites and face-sharing B'_2O9 dimer sites [7–34]. When synthesized under high pressure (HP) of 3–6 GPa, 6*H* Ba3NiSb2O9 and Ba3CuOs2O9 showed atomic rearrangements and the resulting phases can be described as Ba3Sb(NiSb)O9 and Ba3Os(CuOs)O9, respectively, in which the corner-sharing octahedra sites are occupied by pentavalent Sb^{5+}/Os^{5+} ions and the dimer sites are occupied by (NiSb)/(CuOs) [35–37]. Based on such structural features triple perovskite oxides show diverse magnetic properties, such as spin-dimer, antiferromagnetic (AFM), as well as FIM order and possible spin-liquid behavior [9,15,20,23,35,36]. However, triple perovskite oxides with Curie temperatures (T_c) above room temperature have not been reported yet to the best of our knowledge. In this work, triple perovskites Ba3NiOs2O9 were synthesized at ambient pressure (AP) and high-pressure (HP) conditions, respectively. The AP Ba3NiOs2O9 phase shows AFM order at 130 K; surprisingly, the HP Ba3NiOs2O9 displays a weak FM transition with a high T_c of ≈ 400 K and a large hysteresis.

*Corresponding author: hai.feng@iphy.ac.cn
†Corresponding author: is.jiechen@gmail.com

II. EXPERIMENT

The AP $Ba_3NiOs_2O_9$ was synthesized by solid-state reactions from BaO (decomposition of $BaCO_3$, Alfa 99.8%), NiO (Alfa 99%), and Os (Alfa 99.95%) in two steps. First, BaO and Os with a mole ratio of 3 : 2.4 were well ground together and pressed into pellets inside an Ar glovebox. The pellets were then loaded into a corundum crucible, which was placed into a silica tube along with a second corundum crucible containing MnO_2 (Alfa 99.9%). The silica tube was then sealed under the dynamic vacuum using a H_2/O_2 torch, and heated at 750 °C for 48 h. MnO_2 decomposes into $\frac{1}{2}Mn_2O_3 + \frac{1}{4}O_2$ at 550 °C and acts as an oxygen source for the reaction. The molar ratio of Os and MnO_2 applied was 1/5. This synthesis process is similar to that of $Ba_3Os_2O_9$ [38]. Second, the products obtained were mixed with NiO with weight ratios of 1 : 0.0849, corresponding to 1 : 1 molar ratios of $Ba_3Os_2O_9$: NiO. The mixed powders were pressed to pellets and loaded into corundum crucibles which were placed in silica tubes. The silica tubes were sealed under dynamic vacuum and then annealed at 950 °C for 48 h. A similar two-step method was used to synthesize $Ba_3CuOs_2O_9$ and $Ba_3ZnOs_2O_9$ [16].

The HP $Ba_3NiOs_2O_9$ was initially obtained by annealing the AP phase under high pressure. The as prepared AP $Ba_3NiOs_2O_9$ samples were thoroughly ground and sealed into Pt crucibles. The Pt crucibles were then loaded into a multianvil-type press (CTF-MA1500P, C&T Factory Co., Ltd, Japan) with a pressure of 6 GPa. The crucibles were heated at 1100 °C for 30 min while the pressure maintained stable. Then the pressure was released gradually. Subsequently we found that HP $Ba_3NiOs_2O_9$ can be synthesized directly from BaO (decomposition of $BaCO_3$, Alfa 99.8%), NiO (Alfa 99%), OsO_2 (Lab made from Os powder), and $KClO_4$ (Kishida Chemical >99.5%). Powders of BaO, NiO, OsO_2, and $KClO_4$ with a mole ratio of 3 : 1 : 2 : 0.26 were well ground and sealed into a Pt crucible inside an Ar glovebox, which was then loaded into the same multianvil-type press with a pressure of 6 GPa. After heating at 1100 °C for 30 min while maintaining the high pressure, the press released the pressure gradually. The obtained samples were rinsed in deionized water to remove the residual KCl. Samples obtained by these two methods show similar x-ray-diffraction (XRD) patterns and magnetic properties (see Figs. S1–S3 in the Supplemental Material [39]). The properties reported in this paper are measured on the sample synthesized by the latter method. Using the latter method, a total amount of about 3.0 g HP $Ba_3NiOs_2O_9$ was produced for the neutron-diffraction study by repeated sample preparation runs.

A part of the AP $Ba_3NiOs_2O_9$ sample was finely ground for powder x-ray-diffraction (XRD) characterization (Guinier technique, Huber G670 camera, Cu-$K\alpha_1$ radiation, $\lambda = 1.54056$ Å, germanium monochromator, $10° \leqslant 2\theta \leqslant 85°$, the step width was 0.005°). A part of the HP $Ba_3NiOs_2O_9$ sample was thoroughly ground for room-temperature synchrotron x-ray-diffraction (SXRD) measurement at the BL15XU beamline, SPring8, Japan. The refinement of crystal structures was carried out by Rietveld analysis using the RIETAN-VENUS program [40], and the crystal structures were drawn using the VESTA software [41].

Neutron powder-diffraction (NPD) experiments of HP $Ba_3NiOs_2O_9$ were carried out on the instruments E2, E6, and E9 at the BER II reactor of the Helmholtz-Zentrum Berlin. The instrument E9 uses a Ge-monochromator selecting the neutron wavelength $\lambda = 1.308$ Å, while the instruments E2 and E6 use a pyrolytic graphite monochromator selecting the neutron wavelengths $\lambda = 2.38$ and 2.43 Å, respectively. At room-temperature a NPD pattern was recorded on the instrument E9 between the diffraction angles 7.5° and 141.7° to determine the crystal structure parameters of HP $Ba_3NiOs_2O_9$. To study the magnetic long-range ordering, NPD patterns of HP $Ba_3NiOs_2O_9$ were recorded on the instruments E2 and E6. Rietveld refinements of the NPD data were carried out with the program FULLPROF [42]. For the refinements of the NPD data the nuclear scattering lengths $b(O) = 5.805$ fm, $b(Ni) = 10.3$ fm, $b(Ba) = 5.25$ fm, and $b(Os) = 11.0$ fm were used [43].

X-ray-absorption spectroscopy (XAS) and x-ray magnetic circular dichroism (XMCD) spectra at the Ni-$L_{2,3}$ and the Os-$L_{2,3}$ edges were measured at the BL29 BOREAS beamline [44] of ALBA synchrotron (Spain) and at the ODE beamline of Soleil synchrotron (France), respectively. The degree of circular polarization in BOREAS and ODE beamline was close to 100% and 90%, respectively. The Os-$L_{2,3}$ (Ni-$L_{2,3}$) XMCD spectra were measured in a magnetic field of 13 kOe (60 kOe) and at a temperature of 4.5 K (2 K). NiO at the Ni-$L_{2,3}$ edge and Sr_2FeOsO_6 at the Os-L_3 edge were also measured for energy calibration purposes.

Using pieces of as synthesized pellets, the electrical resistivity (ρ) was measured with a DC gauge current of 0.1 mA by the four-point method using a Physical Properties Measurement System (PPMS, Quantum Design, Inc.). Electrical contacts were made with Au wires and silver glue. The temperature dependence of the specific heat (C_p) was measured in the same PPMS apparatus by using its HC option (relaxation method). The magnetic susceptibilities (χ) of the samples were measured in a superconducting quantum interference device magnetometer (MPMS, Quantum Design), at zero-field-cooling (ZFC) and field-cooling (FC) conditions in a temperature range between 2 and 380 K under applied magnetic fields of 10 kOe. The isothermal magnetization curves were measured at 5 K. The high-temperature χ data were measured using the oven accessory for the PPMS.

III. RESULTS

Crystal structures. The XRD pattern of the AP $Ba_3NiOs_2O_9$ phase [see Fig. 1(a)] can be well refined in the hexagonal triple perovskite structure with space group $P6_3/mmc$ (no. 194), which was adapted by most reported triple perovskite oxides [11–14,27,28,31]. In AP $Ba_3NiOs_2O_9$, the Ni occupies the $2a(0, 0, 0)$ site while the Os occupies the $4f(\frac{1}{3}, \frac{2}{3}, z)$ site. The face-sharing Os-centered octahedra form Os_2O_9 dimer units which share corners with NiO_6 octahedra as shown in Fig. 2(a). The detailed crystal parameters, atomic positions, and thermal displacement parameters of AP $Ba_3NiOs_2O_9$ are summarized in Table I.

The SXRD data of HP $Ba_3NiOs_2O_9$ were successfully Rietveld refined with the same space group $P6_3/mmc$ as for the AP phase. Refinement results indicate that the HP
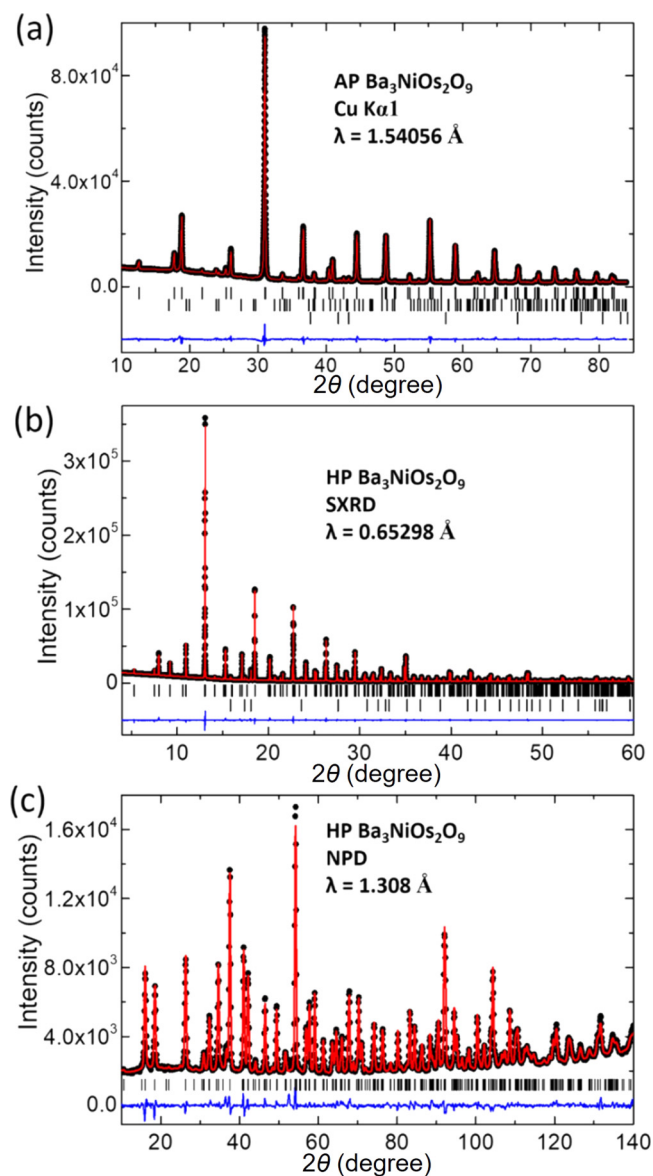
FIG. 1. (a) XRD pattern of AP $Ba_3NiOs_2O_9$, (b) SXRD pattern of HP $Ba_3NiOs_2O_9$, (c) NPD pattern of HP $Ba_3NiOs_2O_9$ at room temperature. The calculated patterns (red) obtained by Rietveld refinement of the experimental patterns in space group $P6_3/mmc$ are compared with the observed data (black dots), and the difference is shown as blue patterns. The vertical black bars are indicating the diffraction positions for the title compound and minor impurity phases ($BaCO_3$ and Os in AP $Ba_3NiOs_2O_9$; Os in SXRD data of HP $Ba_3NiOs_2O_9$).

FIG. 2. The crystal structures of (a) AP $Ba_3NiOs_2O_9$ and (b) HP $Ba_3NiOs_2O_9$.

refinement in $P6_3/mmc$. The refinements results against space group $P6_3mc$ are summarized in Table S1 in the Supplemental Material [39], and indicated that in the $NiOsO_9$ dimers one $2b$ site is slightly Os dominant (occupancy of Ni1/Os2 = 0.46/0.54) whereas the other is slightly Ni-dominant (occupancy of Ni2/Os3 = 0.54/0.46). However, both the differences in R values as well as the differences in occupancies are too small to justify symmetry lowering from $P6_3/mmc$ to $P6_3mc$ for HP $Ba_3NiOs_2O_9$. Accordingly, in the XRD experiment the Ni and Os ions appear to be essentially disordered at the face-sharing sites. The structural situation in HP $Ba_3NiOs_2O_9$ is reminiscent of that in the HP $Ba_3NiSb_2O_9$ [37], where detailed electron-diffraction studies have shown that XRD as well as NPD experiments rather reveal an average structure whereas on smaller length scales full cation order at the face-sharing sites is retained. For HP $Ba_3NiSb_2O_9$ the trigonal space groups $P3m1$ and $P3$ were considered which lead to alternating stacking sequences of face-sharing $NiSbO_9$ dimers. Similarly, in HP $Ba_3NiOs_2O_9$ the average $P6_3/mmc$ structure may correspond to local ordering patterns where the arrangement of $NiOsO_9$ dimers varies in different domains which explains the average occupancies derived from

phase is very different from the AP phase: the corner-sharing octahedra are fully occupied by Os, and the face-sharing octahedra are shared by Ni and Os [see Fig. 2(b)]. To check for possible Ni and Os ordering, we then refined the data with a lower-symmetry space group $P6_3mc$ which was suggested for the HP $Ba_3NiSb_2O_9$ phase [36]. The face-sharing site ($4f$) in space group $P6_3/mmc$ is split into two distinguishable $2b$ sites in $P6_3mc$. Refinement against $P6_3mc$ resulted in $R_{wp} = 2.99\%$ and $R_p = 2.12\%$ which is not a significant improvement compared to $R_{wp} = 3.06\%$ and $R_p = 2.16\%$ from the

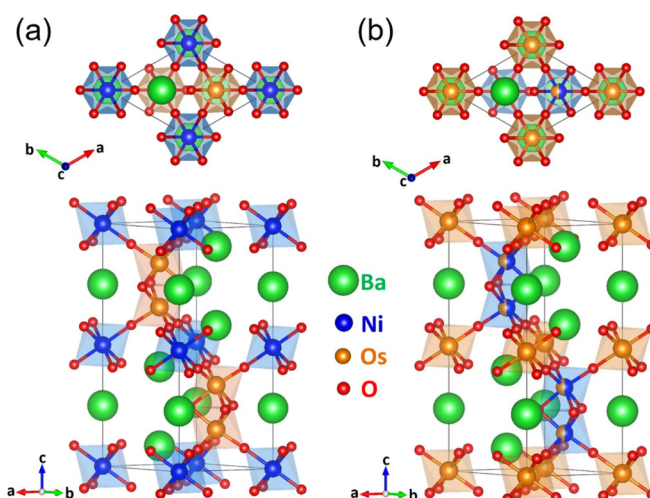TABLE I. Atomic positions and thermal displacement parameters for AP $Ba_3NiOs_2O_9$.[a] During the refinement, B_{iso} for Ba1, Ba2, Ni1, and Os1 were constrained to be equal. B_{iso} for O1 and O2 were constrained to be equal.

Atom	Wyckoff site	x	y	z	B_{iso} (Å^2)
Ba1	$2b$	0	0	$\frac{1}{4}$	0.31(2)
Ba2	$4f$	$\frac{1}{3}$	$\frac{2}{3}$	0.912 72 (5)	0.31(2)
Ni1	$2a$	0	0	0	0.31(2)
Os1	$4f$	$\frac{1}{3}$	$\frac{2}{3}$	0.159 08(4)	0.31(2)
O1	$6h$	0.4863(5)	0.9726	$\frac{1}{4}$	0.17(7)
O2	$12k$	0.1676(4)	0.3352	0.4167(3)	0.17(7)

[a]Space group: $P6_3/mmc$ (no. 194). Cell parameters: $a = 5.761\,73(2)$ Å, $c = 14.065\,22(8)$ Å, $V = 404.374$ Å^3, and $Z = 2$. Residuals: $R_{wp} = 4.41\%$, $R_p = 3.14\%$, $S = 2.73$.

TABLE II. Results of the atomic positions and thermal displacement parameters for HP $Ba_3NiOs_2O_9$ SXRD data refined in space group: $P6_3/mmc$ (no. 194).[a] During the refinement, B_{iso} for Ba1 and Ba2, Os1 and Ni1/Os2, O1 and O2 were constrained to be equal, respectively.

Atom	Wyckoff site	Occupancy	x	y	z	B_{iso} (Å^2)
Ba1	$2b$	1	0	0	$\frac{1}{4}$	0.64(1)
Ba2	$4f$	1	$\frac{1}{3}$	$\frac{2}{3}$	0.906 57(3)	0.64(1)
Os1	$2a$	1	0	0	0	0.18(1)
Ni1/Os2	$4f$	0.5/0.5	$\frac{1}{3}$	$\frac{2}{3}$	0.157 32(3)	0.18(1)
O1	$6h$	1	0.4839(4)	0.9678	$\frac{1}{4}$	0.79(4)
O2	$12k$	1	0.1686(3)	0.3372	0.4190(2)	0.79(4)

[a]Cell parameters: $a = 5.735\,06(1)$ Å, $c = 14.107\,64(1)$ Å, $V = 401.8467(5)$ Å^3, and $Z = 2$. Residuals: $R_{wp} = 3.06\%$, $R_p = 2.16\%$, and $S = 2.16$.

the SXRD data. The Rietveld refined SXRD pattern of HP $Ba_3NiOs_2O_9$ in space group $P6_3/mmc$ is shown in Fig. 1(b); the detailed crystal parameters, atomic positions, and thermal displacement parameters are summarized in Table II. The crystal structure of HP $Ba_3NiOs_2O_9$ was also investigated by neutron diffraction to get more accurate oxygen positions. The room-temperature neutron data were successfully refined in the space group $P6_3/mmc$ [see Fig. 1(c)]. The data were also refined with lower symmetry space group $P6_3mc$, but no significant improvement was observed. The detailed crystal parameters, R values, atomic positions, and thermal displacement parameters are summarized in Tables S2 and S3 in the Supplemental Material [39].

The bond lengths of Ni- and Os-centered octahedra are summarized in Table III. For Ni-centered octahedra in AP $Ba_3NiOs_2O_9$, there are six equal Ni1-O2 bonds with length of 2.042(3) Å, which is comparable to 2.057 Å for $Ba_3NiRu_2O_9$ [26] and 2.040 Å for Ba_2NiWO_6 [45]. For Os-centered octahedra in AP $Ba_3NiOs_2O_9$, there are three longer bonds [Os1-O1 = 1.992(2) Å] and three shorter bonds [Os1-O2 = 1.967(3) Å]. This kind of distortion is commonly observed in oxides having M_2O_9 dimer units, which is presumably due to electrostatic repulsion between the M cations within the M_2O_9 unit [46]. For HP $Ba_3NiOs_2O_9$ the more accurate bond lengths calculated from refinement of NPD data

TABLE III. Selected bond lengths and bond angles for AP and HP $Ba_3NiOs_2O_9$ (space group $P6_3/mmc$). The distances were calculated from XRD data for AP $Ba_3NiOs_2O_9$ and neutron data for HP $Ba_3NiOs_2O_9$ at room temperature, respectively.

AP $Ba_3NiOs_2O_9$		HP $Ba_3NiOs_2O_9$	
Bond	Length/Angle	Bond	Length/Angle
Ni1-O2	2.042(3) Å $\times$ 6	Os1-O2	1.968(2) Å $\times$ 6
Os1-O1	1.992(2) Å $\times$ 3	Ni1/Os2-O1	2.025(2) Å $\times$ 3
Os1-O2	1.967(3) Å $\times$ 3	Ni1/Os2-O2	2.006(2) Å $\times$ 3
Os1-O1-Os1	79.90(6)°	Ni1/Os2-O1-Ni1/Os2	82.3°
Ni1-O2-Os1	177.8(2)°	Os1-O2-Ni1/Os2	178.1°
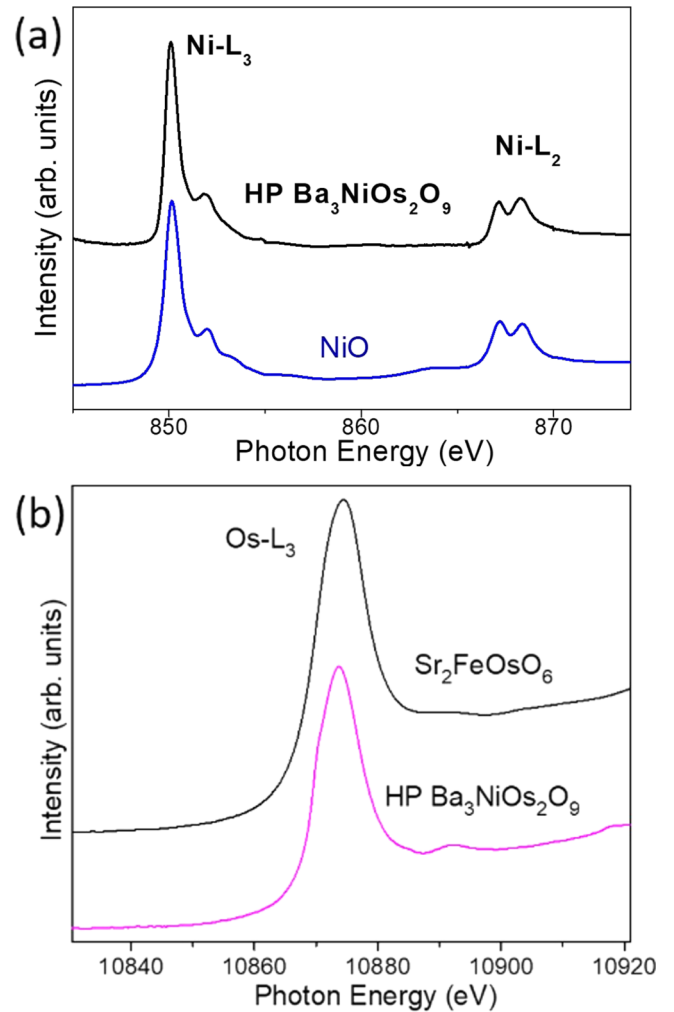
FIG. 3. (a) Ni-$L_{2,3}$ XAS spectra of HP $Ba_3NiOs_2O_9$ and NiO. (b) Os-L_3 XAS spectra of HP $Ba_3NiOs_2O_9$ and Sr_2FeOsO_6 (Os^{5+} reference).

at room temperature are given. The Os1-O bond length is 1.968 Å, in good agreement with the expectations for Os^{5+} [5,47,48], whereas the average Ni1/Os2-O bond length is 2.016 Å which reflects the mixed site occupancy with Ni^{2+} and Os^{5+} ions. To confirm the valence states, HP $Ba_3NiOs_2O_9$ was further investigated by XAS.

X-ray-absorption spectroscopy. XAS spectra at the Ni-$L_{2,3}$ edges are highly sensitive to the valence state, spin orientation, and local environment [49–51]. The identical energy positions and similar multiplet spectral structures of the Ni-$L_{2,3}$ edges of HP $Ba_3NiOs_2O_9$ and NiO demonstrate the same Ni^{2+} valence state [see Fig. 3(a)]. Unlike 3d transition metals with narrow 3d bands, the broad 5d bands give rise to a broad $L_{2,3}$ XAS spectrum and smear multiplet spectral structures, however the energy position of the strong white line (WL) is still sensitive to the valence states of 5d elements [52–56]. The same energy position of the WL in the Os-L_3 XAS spectra of $Ba_3NiOs_2O_9$ and Sr_2FeOsO_6 (Os^{5+} reference) indicates the Os^{5+} valence state in $Ba_3NiOs_2O_9$ fulfilling the charge balance requirement [see Fig. 3(b)].
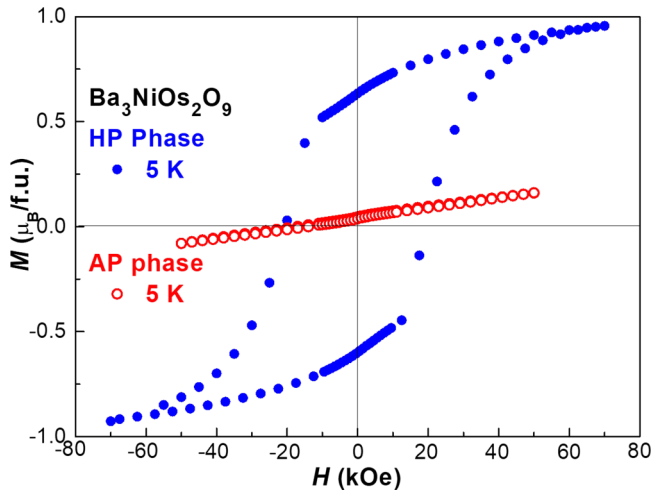
FIG. 4. Isothermal magnetization curves of AP and HP $Ba_3NiOs_2O_9$ at 5 K.

Magnetic properties. Isothermal magnetization $M(H)$ data of HP $Ba_3NiOs_2O_9$ are very different from those of the AP phase as shown in Fig. 4. At 5 K the AP phase shows roughly linear $M(H)$ behavior, but the HP phase shows a FM hysteresis with a large coercive field (20.2 and 26.3 kOe for the two different samples of HP $Ba_3NiOs_2O_9$; see Fig. S3 [39]) and without saturation of the magnetization up to 7 T.

The temperature dependence of both the ZFC and FC magnetic susceptibility curves of AP $Ba_3NiOs_2O_9$ (Fig. 5) shows a kink at 133 K, indicating a magnetic phase transition. The linear $M(H)$ behavior at 5 K (see Fig. 4) as well as the small susceptibility values are in agreement with an AFM transition, which was further supported by the specific-heat data revealing a λ-type anomaly around 130 K as shown in the inset of Fig. 5. Neither the ZFC nor the FC data above the transition temperature can be fitted with a Curie-Weiss (CW) law. The ZFC and FC curves start to deviate from each other around 280 K. The origin of this effect is not clear, but it could
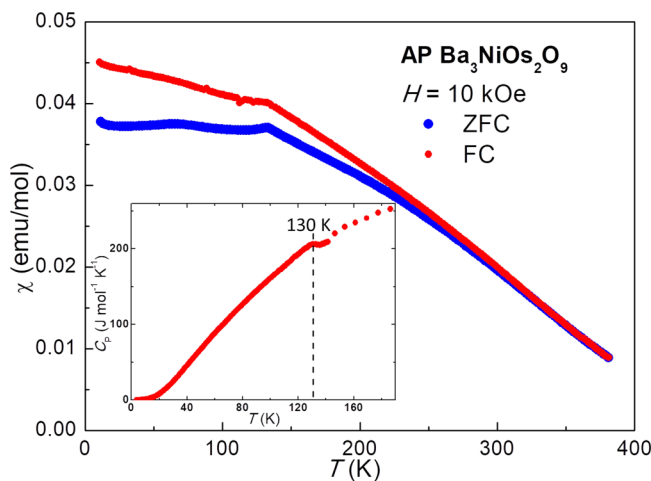

FIG. 5. Temperature dependence of magnetic susceptibility of AP $Ba_3NiOs_2O_9$. The inset shows the temperature dependence of the specific heat of AP $Ba_3NiOs_2O_9$.

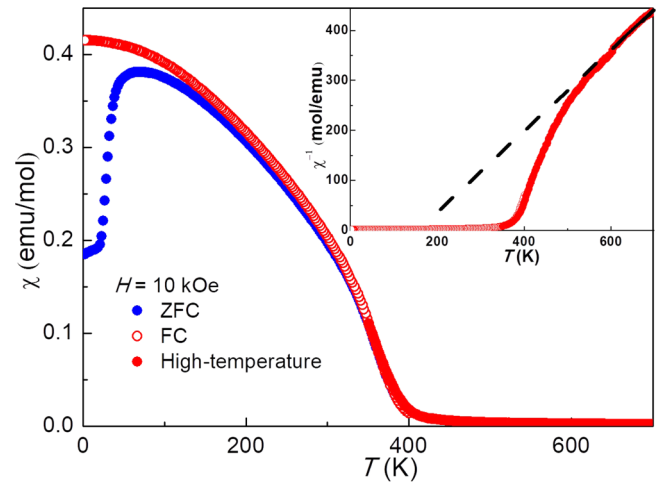
FIG. 6. Temperature dependence of the magnetic susceptibility of HP $Ba_3NiOs_2O_9$. The upper inset shows the corresponding χ^{-1} vs T data.

be due to a weak ferromagnetic component introduced by a small degree of antisite disorder.

The temperature-dependent magnetic susceptibility data of HP $Ba_3NiOs_2O_9$ show a sharp increase below 400 K with cooling (see Fig. 6), indicating a FM or FIM order. Even above 400 K there are pronounced deviations from linearity in the inverse susceptibility $\chi^{-1}(T)$. CW analysis of the 600–700-K data results in a positive Weiss temperature (θ_w) of 131 K, and an effective moment (μ_{eff}) per formula unit of 3.23 μ_B. Using the spin-only moment of Ni^{2+}, 2.83 μ_B, and the average Os^{5+} moment, 3.28 μ_B, obtained for other Os^{5+} compounds [47,48,57–59] one calculates an expected effective moment of 5.43 μ_B/f.u. for $Ba_3NiOs_2O_9$. The experimental μ_{eff} is much smaller than the calculated one which is attributed to the persistence of strong Os^{5+}-O-Os^{5+} AF correlations between the corner-sharing units above T_c which leads to cancellation of the Os moments (see the Discussion section). The positive θ_w indicates that overall FM couplings determine the magnetic order in HP $Ba_3NiOs_2O_9$. The magnetization of HP $Ba_3NiOs_2O_9$ was 0.95 μ_B/f.u. at 5 K and 70 kOe (1.09 μ_B/f.u. for the other sample prepared by conversion of AP into HP $Ba_3NiOs_2O_9$; see Fig. S3). Taking into account the spin-only moments of Ni^{2+} ($t_{2g}^6 e_g^2$) (giving 2 μ_B) and Os^{5+} (t_{2g}^3) (giving $2 \times 3 = 6 \mu_B$), a truly FM $Ba_3NiOs_2O_9$ would have a theoretical saturation magnetization of 8.0 μ_B/f.u., which is much larger than the moment obtained from the magnetization measurements. Thus, the magnetic order of HP $Ba_3NiOs_2O_9$ is referred to as weak FM, which is attributed to strong AFM Os^{5+}-Os^{5+} interactions as suggested by the XMCD data presented in the following.

X-ray magnetic circular dichroism. The XMCD spectra for HP $Ba_3NiOs_2O_9$, reported in Fig. 7, were measured below T_c in an applied field. The Ni-$L_{2,3}$ XMCD and Os-$L_{2,3}$ XMCD signals have the same sign, which indicates a parallel coupling between Ni and Os moments, and supports a weak FM ground state. By applying the spin and orbital sum rules to the Os-$L_{2,3}$ XMCD spectrum, we estimate the orbital and spin moments of Os^{5+} to be $m_l = 0.0006 \mu_B$ and $m_s = 0.008 \mu_B$. The total moment is then 0.0086 μ_B per Os^{5+} ion. Applying the sum
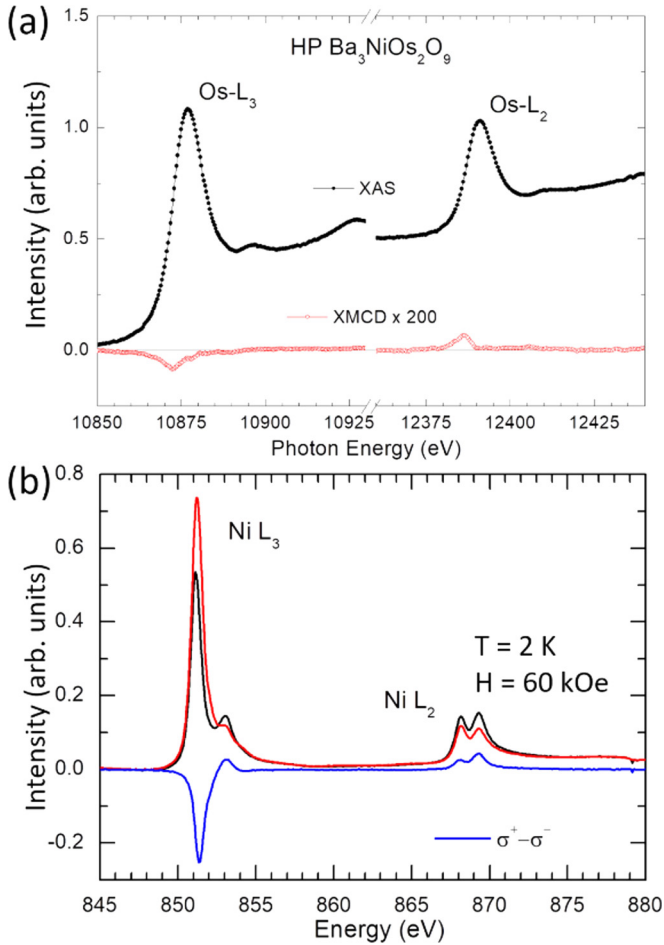
FIG. 7. (a) XMCD spectra at Os-*L* edges of Ba$_2$NiOs$_2$O$_9$ measured at 4.5 K and 13 kOe. (b) XMCD spectra at Ni *L* edges of Ba$_3$NiOs$_2$O$_9$ measured at 2 K and 60 kOe.

rules to the Ni-$L_{2,3}$ XMCD spectra gives an estimated net magnetic moment of 0.81 μ_B/Ni atom ($m_s = 0.655\,\mu_B$ and $m_l = 0.154\,\mu_B$), which is comparable to the total magnetization of 0.95 μ_B measured at 70 kOe. Note that in the application of the sum rules the intrinsic dipole moment T_z was considered to be negligible for both ions, as expected for d^3 (half-filled t_{2g} shell) and d^8 (half-filled e_g shell) ions in a high-spin state.

Magnetic structure. In order to investigate in more detail the magnetic structure of HP Ba$_3$NiOs$_2$O$_9$ we carried out a NPD study on the instruments E2 and E6 at 2 K. At first sight we could not find evidence for long-range magnetic ordering. In the case of a FIM or FM ordering magnetic intensities are expected to appear on the positions of nuclear Bragg reflections, but weak magnetic intensities are difficult to observe at the strong nuclear Bragg reflections 101, 102, and the pair 104/110. A closer inspection revealed a magnetic contribution to the weak nuclear reflection 100 (see Fig. 8). On the other hand, no magnetic intensity was observed at the weak nuclear reflections 002, 004, and 103. This indicates that the ordered magnetic moments are predominantly aligned parallel to the hexagonal *c* axis. In space group $P6_3/mmc$ there are two Wyckoff sites that accommodate transition metal ions: the 2*b* site is fully occupied by Os1, while the 4*f* site
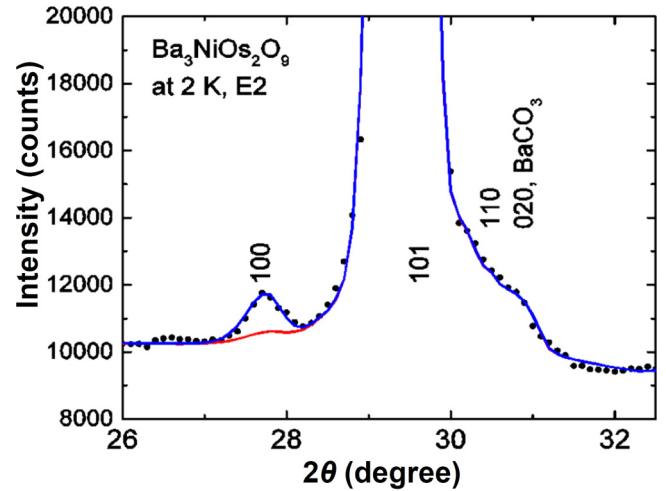

FIG. 8. NPD pattern of HP Ba$_3$NiOs$_2$O$_9$ collected on instrument E2 at 2 K ($\lambda = 2.38\,\text{Å}$). The calculated pattern of the nuclear structure (red) is compared with the calculated one, where the superimposed magnetic ordering is also taken into account. Further, both patterns are compared with the experimental pattern (black dots). The positions of two reflections of the impurity phase BaCO$_3$ are also marked.

is statistically occupied by Ni and Os (labeled as Ni1/Os2). Considering the XMCD results we refined the data with a pure FM model, where the Os moments at the pure Os sublattice and the Os at the mixed sublattice is equal to zero. Then one obtains for the Ni atoms at the mixed sites and accordingly for the total FM moment a value of 1.6(2) μ_B at 2 K which is somewhat larger than the moment values at 2 K obtained from the magnetization and XMCD measurements at 70 and 60 kOe, respectively.

Due to the fact that only for the reflection 100 a weak magnetic intensity was found it is not possible to determine the magnetic structure unambiguously. Furthermore, as discussed above, the $P6_3/mmc$ structure may correspond to an average structure being composed of lower-symmetry domains, which would also result in an average magnetic structure.

IV. DISCUSSION

Polycrystalline samples of Ba$_3$NiOs$_2$O$_9$ have been synthesized under AP and HP conditions, respectively. The AP and HP Ba$_3$NiOs$_2$O$_9$ samples show drastically different magnetic properties which is obviously related to the different cation arrangements in the two phases. As both the AP and HP Ba$_3$NiOs$_2$O$_9$ are electrically semiconducting (see Fig. S4 in the Supplemental Material [39]), the magnetic properties are determined by superexchange interactions between the localized *d* electrons. The AP Ba$_3$NiOs$_2$O$_9$ crystallizes in the 6*H* perovskite structure with space group $P6_3/mmc$, where the Os atoms occupy the face-sharing octahedral sites forming Os$_2$O$_9$ dimer units and Ni atoms sit at the corner-sharing octahedral site forming NiO$_6$ octahedra. The antiferromagnetism with $T_N \approx 130\,\text{K}$ of AP Ba$_3$NiOs$_2$O$_9$ is comparable to that of similar ruthenates, Ba$_3$NiRu$_2$O$_9$, Ba$_3$CoRu$_2$O$_9$, and Ba$_3$CuRu$_2$O$_9$, which display AFM orders at 90, 90, and 100 K, respectively. The magnetic properties are believed

to be dominated by the $3d$ transition metal in these triple perovskite oxides [20,26,27], because the Ru_2O_9 and Os_2O_9 units tend to form nonmagnetic spin-gapped singlet dimers as in $Ba_3ZnOs_2O_9$ [16] and $Ba_3MRu_2O_9$ (M = Ca, Zn, and Bi) [23,29,33]. The susceptibility data of $Ba_3ZnOs_2O_9$ and $Ba_3ZnRu_2O_9$ show weakly temperature-dependent behavior [16,33].

When the AP $Ba_3NiOs_2O_9$ sample is annealed under HP conditions, the atoms are rearranged. Alternatively, the HP phase can be directly synthesized from the oxides in a press. In HP $Ba_3NiOs_2O_9$ the space group $P6_3/mmc$ appears to be preserved, but the corner-sharing site is now fully occupied by Os, whereas the face-sharing octahedral sites appear to be occupied by both Ni^{2+} and Os^{5+} ions. However, like in $Ba_3NiSb_2O_9$ [37], on a smaller length scale than probed by XRD and NPD experiments, Ni^{2+}-Os^{5+} ordering in the face-sharing dimers may still occur and the apparent $P6_3/mmc$ space group may rather reflect an average of domains. Compared with the AP phase, HP $Ba_3NiOs_2O_9$ shows a reduced volume per formula unit, V/Z: The V/Z is 200.923 $Å^3$ for HP $Ba_3NiOs_2O_9$, which is 0.6% smaller than that of 202.187 $Å^3$ for the AP phase. The atomic rearrangement in HP $Ba_3NiOs_2O_9$ thus leads to a denser phase. High-pressure conditions generally stabilize crystal structures of higher density, for instance in the case of $BaIrO_3$ [60,61]: $BaIrO_3$ synthesized at AP crystallizes in the 9R structure (V/Z = 70.89 $Å^3$), in the 5H structure when synthesized at 4 GPa (V/Z = 68.88 $Å^3$), in the 6H structure when synthesized at 5 GPa (V/Z = 68.34 $Å^3$), and in the 3C structure when synthesized at 25 GPa (V/Z = 65.825). Furthermore, the AP structure of $Ba_3NiOs_2O_9$ with both Os^{5+} ions on the face-sharing sites may became instable under pressure due to strong electrostatic repulsion which may be reduced by accommodation of Ni^{2+} and Os^{5+} ions on the face-sharing and Os^{5+} on the corner-sharing sites.

The bond angles of the superexchange paths are 82.3° between face-sharing sites and 178.1° between corner-sharing sites. The magnetic properties of HP $Ba_3NiOs_2O_9$ are expected to be dominated by the interactions between corner-sharing octahedral sites, namely Os-O-Ni/Os and Os-O-Os/Ni interactions. As Os^{5+} has the $5d^3$ (t_{2g}^3) electronic configuration, the Os^{5+}-O-Os^{5+} couplings are expected to be strongly AFM according to the Goodenough-Kanamori (GK) rules [62], which is also evidenced by the high T_N of $NaOsO_3$ [63,64]. These correlations possibly persist above T_c which is the reason for the small μ_{eff} obtained from CW analysis. However, the positive θ_w indicates that FM interactions determine the magnetic order in HP $Ba_3NiOs_2O_9$, which implies that the Os^{5+}-O-Ni^{2+} couplings must be FM. The d^8−d^3 interactions via ∼180° superexchange path are indeed expected to be FM according to the GK rules [62] which is due to virtual hopping from the half-filled e_g orbitals of Ni^{2+} ($t_{2g}^6 e_g^2$) to the empty e_g orbitals of Os^{5+} ($t_{2g}^3 e_g^0$). The XMCD data support a FM coupling of Ni and Os moments. Due to the strong AFM Os^{5+}-O-Os^{5+} interactions, the Os moments are almost compensated, which is in agreement with the fact that in our XMCD data only a small but finite net moment ≈0.008 μ_B is observed for Os. In the case of perfect cation order in the triple perovskite $Ba_3Os^{5+}(Ni^{2+}Os^{5+})O_9$ above interactions should give rise to a FM alignment of Ni^{2+}

spins with an expected spin-only moment of 2μ_B. The net moment of 0.81 μ_B for Ni^{2+} from the XMCD data is much smaller than 2 μ_B, indicating either incomplete alignment of the magnetic domains at the measurement field of 60 kOe or partial compensation of the Ni moments. The latter could arise from a disordered arrangement of Os and Ni ions on the face-sharing sites as implied by the XRD and NPD experiments which would change the exchange interaction pattern. For instance, Ni-Ni AFM interactions via the ∼90° superexchange path in dimer units could reduce the apparent Ni moments. Microstructural studies are required to clarify the detailed origin of the reduced Ni^{2+} moments.

The large magnetic ordering temperature of 400 K for HP $Ba_3NiOs_2O_9$ is remarkable as due to the enhanced crystal-field splitting at the Os^{5+} sites the FM $3d(e_g^2)$-$5d(e_g^0)$ exchange pathway is expected to be considerably weaker compared to corresponding $3d$-$3d$ interactions [65]. The high T_c probably reflects the peculiar electronic situation in insulators being composed of a strongly correlated $3d$ and a weakly correlated $5d$ element [66]. In addition, spin-orbit coupling may play a role for the magnetism even in Os^{5+} systems with a $5d^3$ (t_{2g}^3) electron configuration [67].

V. CONCLUSIONS

Polycrystalline samples of $Ba_3NiOs_2O_9$ were synthesized at AP and HP conditions, respectively. Both samples are electrically semiconducting. The AP $Ba_3NiOs_2O_9$ crystallizes in the 6H perovskite structure with space group $P6_3/mmc$, consisting of face-sharing Os_2O_9 dimer units and corner-sharing NiO_6 octahedra. AP $Ba_3NiOs_2O_9$ shows AFM order below 130 K, in which the magnetic properties are dominated by Ni^{2+} ions. HP $Ba_3NiOs_2O_9$ crystallizes in the 6H perovskite structure too but the face-sharing octahedral sites appear to be occupied by both, Ni^{2+} and Os^{5+} ions, whereas the corner-sharing site is occupied exclusively by Os^{5+}. However, on a more local scale than probed by XRD and NPD experiments ordered $NiOsO_9$ dimers may occur. HP $Ba_3NiOs_2O_9$ displays a high-T_c (≈ 400 K) weak FM transition, which is much different from the antiferromagnetism of the AP phase. The long-range magnetic order of HP $Ba_3NiOs_2O_9$ was confirmed by NPD, and XMCD analysis supported FM coupling between Os and Ni moments which leads to a spin arrangement, where the FM moments mainly arise from Ni^{2+} ions.

[1] A. P. Ramirez, J. Phys.: Condens. Matter **9**, 8171 (1997).

[2] C. N. R. Rao, Annu. Rev. Phys. Chem. **40**, 291 (1989).

[3] W. Witczak-Krempa, G. Chen, Y. B. Kim, and L. Balents, Annu. Rev. Condens. Matter Phys. **5**, 57 (2014).

[4] Y. Krockenberger, K. Mogare, M. Reehuis, M. Tovar, M. Jansen, G. Vaitheeswaran, V. Kanchana, F. Bultmark, A. Delin *et al.*, Phys. Rev. B **75**, 020404(R) (2007).

[5] H. L. Feng, M. Arai, Y. Matsushita, Y. Tsujimoto, Y. Guo, C.I. Sathish, X. Wang, Y.-H. Yuan, M. Tanaka *et al.*, J. Am. Chem. Soc. **136**, 3326 (2014).

[6] K. L. Kobayashi, T. Kimura, H. Sawada, K. Terakura, and Y. Tokura, Nature (London) **395**, 677 (1998).

[7] P. E. R. Blanchard, K. W. Chapman, S. M. Heald, M. Zbiri, M. R. Johnson, B. J. Kennedy, and C. D. Line, Inorg. Chem. **55**, 5649 (2016).

[8] P. E. R. Blanchard, Z. Huang, B. J. Kennedy, S. Liu, W. Miiller, E. Reynold, Q. Zhou, M. Avdeev, Z. Zhang, J. B. Aitken *et al.*, Inorg. Chem. **53**, 952 (2014).

[9] G. Chen, M. Hermele, and L. Radzihovsky, Phys. Rev. Lett. **109**, 016402 (2012).

[10] T. Dey, R. Kumar, A. V. Mahajan, S. D. Kaushik, and V. Siruguri, Phys. Rev. B **89**, 205101 (2014).

[11] Y. Doi and Y. Hinatsu, J. Solid State Chem. **177**, 3239 (2004).

[12] Y. Doi and Y. Hinatsu, J. Phys.: Condens. Matter **16**, 2849 (2004).

[13] Y. Doi, Y. Hinatsu, Y. Shimojo, and Y. Ishii, J. Solid State Chem. **161**, 113 (2001).

[14] Y. Doi, K. Matsuhira, and Y. Hinatsu, J. Solid State Chem. **165**, 317 (2002).

[15] B. Fak, S. Bieri, E. Canevet, L. Messio, C. Payen, M. Viaud, C. Guillot-Deudon, C. Darie, J. Ollivier, and P. Mendels, Phys. Rev. B **95**, 060402(R) (2017).

[16] H. L. Feng and M. Jansen, J. Solid State Chem. **258**, 776 (2018).

[17] I. Fernandez, R. Greatrex, and N. N. Greenwood, J. Solid State Chem. **34**, 121 (1980).

[18] Z. X. Huang, M. Avdeev, B. J. Kennedy, K. S. Knight, Q. D. Zhou, and C. D. Ling, J. Phys.: Condens. Matter **26**, 276003 (2014).

[19] P. Kohl and D. Reinen, Z. Anorg. Allg. Chem. **433**, 81 (1977).

[20] P. Lightfoot and P. D. Battle, J. Solid State Chem. **89**, 174 (1990).

[21] C. D. Ling, Z. Huang, B. J. Kennedy, S. Rols, M. R. Johnson, M. Zbiri, S. A. J. Kimber, J. Hudspeth, D. T. Adroja, K. C. Rule *et al.*, Phys. Rev. B **94**, 174401 (2016).

[22] Y. Liu, R. L. Withers, V. Ting, J. D. FitzGerald, and L. Noren, Physica B **385**, 564 (2006).

[23] W. Miiller, M. Avdeev, Q. D. Zhou, A. J. Studer, B. J. Kennedy, G. J. Kearley, and C. D. Ling, Phys. Rev. B **84**, 220406(R) (2011).

[24] A. Nag, S. Bhowal, F. Bert, A. D. Hillier, M. Itoh, I. Carlomangno, C. Meneghini, T. Sarkar, R. Mathieu, I. Dasgupta *et al.*, Phys. Rev. B **97**, 064408 (2018).

[25] J. A. Quilliam, F. Bert, A. Manseau, C. Darie, C. Guillot-Deudon, C. Payen, C. Baines, A. Amato, and P. Mendels, Phys. Rev. B **93**, 214432 (2016).

[26] J. T. Rijssenbeek, Q. Huang, R. W. Erwin, H. W. Zandbergen, and R. J. Cava, J. Solid State Chem. **146**, 65 (1999).

[27] J. T. Rijssenbeek, P. Matl, B. Batlogg, N. P. Ong, and R. J. Cava, Phys. Rev. B **58**, 10315 (1998).

[28] T. Sakamoto, Y. Doi, and Y. Hinatsu, J. Solid State Chem. **179**, 2595 (2006).

[29] M. S. Senn, A. M. Arevalo-Lopez, T. Saito, Y. Shimakawa, and J. P. Attfield, J. Phys.: Condens. Matter **25**, 496008 (2013).

[30] Y. Shirata, H. Tanaka, T. Ono, A. Matsuo, K. Kindo, and H. Nakano, J. Phys. Soc. Jpn. **80**, 093702 (2011).

[31] K. E. Stitzer, A. El Abed, M. D. Smith, M. J. Davis, S. J. Kim, J. Darriet, and H. C. zur Loye, Inorg. Chem. **42**, 947 (2003).

[32] K. E. Stitzer, M. D. Smith, W. R. Gemmill, and H. C. zur Loye, J. Am. Chem. Soc. **124**, 13877 (2002).

[33] I. Terasaki, T. Igarashi, T. Nagai, K. Tanabe, H. Taniguchi, T. Matsushita, N. Wada, A. Takata, T. Kida, M. Hagiwara *et al.*, J. Phys. Soc. Jpn. **86**, 033702 (2017).

[34] J. Wilkens and H. Mullerbuschbaum, Z. Anorg. Allg. Chem. **619**, 517 (1993).

[35] J. Chen, H. L. Feng, Y. Matsushita, A. A. Belik, Y. Tsujimoto, Y. Katsuya, M. Tanaka, M. X. Wu, M. R. Li, R. F. Zhou *et al.*, J. Solid State Chem. **272**, 182 (2019).

[36] J. G. Cheng, G. Li, L. Balicas, J. S. Zhou, J. B. Goodenough, C. K. Xu, and H. D. Zhou, Phys. Rev. Lett. **107**, 197204 (2011).

[37] C. Darie, C. Lepoittevin, H. Klein, S. Kodjikian, P. Bordet, C. V. Colin, O. I. Lebedev, C. Deudon, and C. Payen, J. Solid State Chem. **237**, 166 (2016).

[38] H. L. Feng, C. Geibel, and M. Jansen, J. Solid State Chem. **249**, 15 (2017).

[39] See Supplemental Material at http://link.aps.org/supplemental/10.1103/PhysRevMaterials.4.064420 for comparison of XRD and magnetic data of HP $Ba_3NiOs_2O_9$ synthesized by two different methods; detailed refinements results of SXRD data of HP $Ba_3NiOs_2O_9$ against space group $P6_3mc$; detailed refinements results of neutron data of HP $Ba_3NiOs_2O_9$ against space group $P6_3/mmc$ and $P6_3mc$; electrical resistivity of AP and HP $Ba_3NiOs_2O_9$.

[40] F. Izumi and T. Ikeda, Mater. Sci. Forum **321-324**, 198 (2000).

[41] K. Momma and F. Izumi, J Appl Crystallogr. **41**, 653 (2008).

[42] J. Rodriguez-Carvajal, Physica B **192**, 55 (1993).

[43] V. F. Sears, in *International Tables for Crystallography*, edited by A. J. C. Wilson (Kluwer, Dordrecht, 1995), Vol. C, p. 383.

[44] A. Barla, J. Nicolás, D. Cocco, S. M. Valvidares, J. Herrero-Martín, P. Gargiani, J. Moldes, C. Ruget, E. Pellegrin, and S. Ferrera, J. Synchrotron Radiat. **23**, 1507 (2016).

[45] S. Nomura and T. Kawakubo, J. Phys. Soc. Jpn. **17**, 1771 (1962).

[46] K. R. Poeppelmeier, A. J. Jacobson, and J. M. Longo, Mater. Res. Bull. **15**, 339 (1980).

[47] H. L. Feng, C. I. Sathish, J. Li, X. Wang, and K. Yamaura, Phys. Procedia **45**, 117 (2013).

[48] H. L. Feng, K. Yamaura, L. H. Tjeng, and M. Jansen, J. Solid State Chem. **243**, 119 (2016).

[49] Z. Hu, M. S. Golden, J. Fink, G. Kaindl, S. A. Warda, D. Reinen, P. Mahadevan, and D. D. Sarma, Phys. Rev. B **61**, 3739 (2000).

[50] M. W. Haverkort, S. I. Csiszar, Z. Hu, S. Altieri, A. Tanaka, H. H. Hsieh, H.-J. Lin, C. T. Chen, T. Hibma, and L. H. Tjeng, Phys. Rev. B **69**, 020408(R) (2004).

[51] H. Guo, Z. W. Li, L. Zhao, Z. Hu, C. F. Chang, C. Y. Kuo, W. Schmidt, A. Piovano, T. W. Pi, O. Sobolev *et al.*, Nat. Commun. **9**, 43 (2018).

[52] S. Agrestini, K. Chen, C.-Y. Kuo, L. Zhao, H.-J. Lin, C.-T. Chen, A. Rogalev, P. Ohresser, T. S. Chan, S. C. Weng, G. Auffermann, A. Volzke, A. C. Komarek, K. Yamaura, M. W. Haverkort, Z. Hu, and L. H. Tjeng, Phys. Rev. B **100**, 014443 (2019).

[53] S. Agrestini, C.-Y. Kuo, K. Chen, Y. Utsumi, D. Mikhailova, A. Rogalev, F. Wilhelm, T. Forster, A. Matsumoto, T. Takayama *et al.*, Phys. Rev. B **97**, 214436 (2018).

[54] H. Deng, M. Liu, J. Dai, Z. Hu, C. Kuo, Y. Yin, J. Yang, X. Wang, Q. Zhao, Y. Xu *et al.*, Phys. Rev. B **94**, 024414 (2016).

[55] X. Wang, M Liu, X. Shen, Z. Liu, Z. Hu, K. Chen, P. Ohresser, L. Nataf, F. Baudelet, H.-J. Lim *et al.*, Inorg. Chem. **58**, 320 (2019).

[56] H. L. Feng, S. Calder, M. P. Ghimire, Y.-H. Yuan, Y. Shirako, Y. Tsujimoto, Y. Matsushita, Z. Hu, C.-Y. Kuo, L. H. Tjeng *et al.*, Phys. Rev. B **94**, 235158 (2016).

[57] A. K. Paul, A. Sarapulova, P. Adler, M. Reehuis, S. Kanungo, D. Mikhailova, W. Schnelle, Z. W. Hu, C. Y. Kuo, V. Siruguri *et al.*, Z. Anorg. Allg. Chem. **641**, 197 (2015).

[58] E. Kermarrec, C. A. Marjerrison, C. M. Thompson, D. D. Maharaj, K. Levin, S. Kroeker, G. E. Granroth, R. Flacau, Z. Yamani, J. E. Greedan, and B. D. Gaulin, Phys. Rev. B **91**, 075133 (2015).

[59] H. L. Feng, M. Reehuis, P. Adler, Z. W. Hu, M. Nicklas, A. Hoser, S. C. Weng, C. Felser, and M. Jansen, Phys. Rev. B **97**, 184407 (2018).

[60] J.-G. Cheng, J. A. Alonso, E. Suard, J.-S. Zhou, and J. B. Goodenough, J. Am. Chem. Soc. **131**, 7461 (2009).

[61] J.-G. Cheng, T. Ishii, H. Kojitani, K. Matsubayashi, A. Matsuo, X. Li, Y. Shirako, J.-S. Zhou, J. B. Goodenough, C. Q. Jin *et al.*, Phys. Rev. B **88**, 205114 (2013).

[62] J. B. Goodenough, *Magnetism and the Chemical Bond* (Interscience-Wiley, New York, 1963).

[63] Y. G. Shi, Y. F. Guo, S. Yu, M. Arai, A. A. Belik, A. Sato, K. Yamaura, E. Takayama-Muromachi, H. F. Tian, H. X. Yang *et al.*, Phys. Rev. B **80**, 161104(R) (2009).

[64] S. Calder, V. O. Garlea, D. F. McMorrow, M. D. Lumsden, M. B. Stone, J. C. Lang, J. W. Kim, J. A. Schlueter, Y. G. Shi, K. Yamaura *et al.*, Phys. Rev. Lett. **108**, 257209 (2012).

[65] Y. S. Hou, H. J. Xiang, and X. G. Gong, Sci. Rep. **5**, 13159 (2015).

[66] O. N. Meetei, O. Erten, M. Randeria, N. Trivedi, and P. Woodward, Phys. Rev. Lett. **110**, 087203 (2013).

[67] A. E. Taylor, R. Morrow, M. D. Lumsden, S. Calder, M. H. Upton, A. I. Kolesnikov, M. B. Stone, R. S. Fishman, A. Paramekanti, P. M. Woodward, and A. D. Christianson, Phys. Rev. B **98**, 214422 (2018).